# Visualization of the Flow around a Circular Cylinder with Tangential Injection

by

Fumio YOSHINO* and Ryoji WAKA*

In this paper, we report the results that were those of the flow visualization around a circular cylinder with tangential injection of water submerged in uniform flow. The visualization technique is the dyefilament method. It is the main object to investigate the behavior of the vortices formed on the surface of the circular cylinder and the side–wall, and shed into the wake of the cylinder. It was found that three kinds of vortices were formed near the juncture of the cylinder and the side–wall, which are quite consistent with the inference from the experiment ¦in the low speed wind tunnel in our laboratry.

## 1   Introduction

We had already described[1] that there was a secondary flow caused by a strong vortex shed from the surface of the cylinder into the wake. Therefore, it was thought that the flow around the cylinder was no longer two-dimensional but three-dimensional near the side-wall. It was not found so far, however, how this vortex was formed and behaved in the wake of the cylinder, that is, the fine structure of the vortex system was not clear. Moreover, it is very difficult to quantitatively analyze such a complex flow obtained in the wind tunnel[2].

Then, we designed and constructed a water tunnel for visualization of the three-dimensional flow of the kind mentioned above.

In this paper, we first describe the water tunnel and second present some photographs of the flow around a cylinder with tangential injection of water. The flow was visualized by means of the dyefilament method.

## 2   Nomenclatures

$X$, $Y$ and $Z$ = Coordinate axes (see Fig. 5) ;
$h$    = Width of the slot ;
$D$   = Diameter of the cylinder ;

* Department of Mechanical Engineering

$\theta$    = Angle measured clockwise from the leading edge ;

$\theta_J$    = Angular position of the slot ;

$U_\infty$    = Uniform velocity in the water tunnel ;

$M$    = Momentum of jet at the outlet of the slot ;

$C_\mu$    = Momentum coefficient of the jet $\left( = \dfrac{Mh}{\dfrac{1}{2}\rho U_\infty^2 D} \right)$ ;

$R_e$    = Reynolds number $\left( = \dfrac{U_\infty D}{\nu} \right)$ ;

$\rho$ and $\nu$ = Density and kinematic viscosity coefficient of water, respectively.

## 3  Experimental apparatus

The water tunnel had been designed by us, constructed by the employee of the university.

The water, stored in the tank on the roof of our laboratory, flows into the water tunnel after passing through a main valve and two flow meters. After that, it in turn passes a submerged weir, two nylon screens of which mesh is 100 or the percentage of voids is 0. 703, a nozzle and a test-section.

Fig. 1 shows the water tunnel. The test-section of the square cross section has the dimensions 200$mm$ in width and depth and 600$mm$ in height, and the four side-walls are made of the transparent acylic-resin plates which are 10$mm$ in thickness. It is a feature of this water tunnel that the water flows vertically from the bottom to the top of the test-section.

(1)  Submerged weir
(2)  Two nylon screens
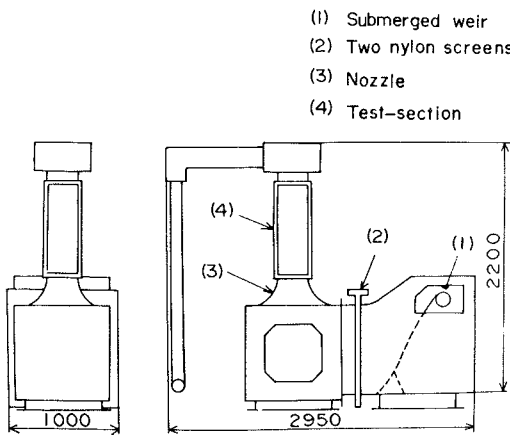(3)  Nozzle
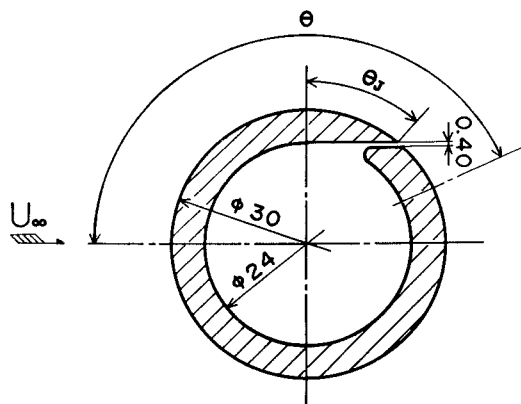(4)  Test—section



Fig. 1.  Water tunnel.

Fig. 2.  Cross section of the model cylinder.

Fig. 2 shows the cross section of the cylinder used in this experiment. The model cylinder is hollow one which has dimensions 30$mm$ in outer diameter, 24$mm$ in inner

diameter and 200*mm* in spanwise length. The water jet is injected along the surface of the cylinder from the slot. This slot has a constant width of 0.4*mm* over the whole span (see Fig. 3).

The circular cylinder can be rotated circumferentially, so that the slot can be fixed at any angular position. The water used for the jet is supplied into the inside of the cylinder from one end of it, so that it may be possible for the jet to have a spanwise velocity component. To eliminate this, many fan-shaped plates are inserted inside of the cylinder and these plates are set perpendicular to the cylinder axis at about equal spanwise space. Their size becomes gradually larger according as the water flows downstream inside the cylinder (see Fig. 3).

we used three kinds of dyes as tracer, that is, they are methylen blue (blue), rhodamine B (red) and fluorescein (green). These dyes are forced out into the uniform flow through the comb-shaped eighteen-nozzle rake that is made of stainless steel pipes of 1.0*mm* in diameter at 10*mm* intervals (see Fig. 4).
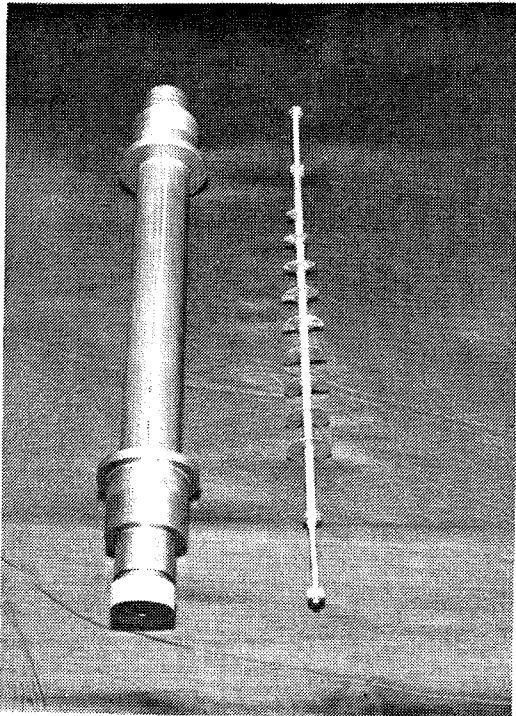


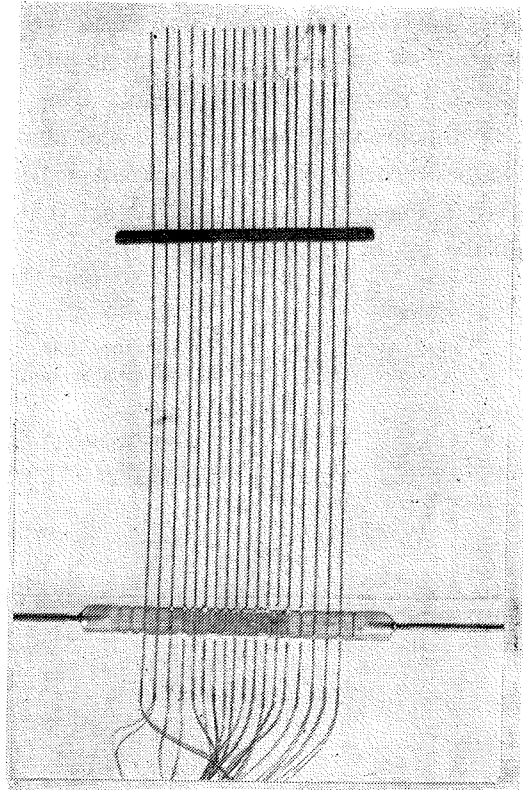Fig. 3.  Model cylinder and fan-shaped
plates.



Fig. 4.  Comb-shaped eighteen-nozzle rake.

## 4  Experimental method

We carried out the calibration of the water tunnel in the first place. It was found by means of the dyefilament method that the flow in the test-section was laminar in the velocity range between 0 *mm*/s and 90 *mm*/s. The velocity distribution of the flow in the test-section was examined in the above-mentioned velocity range by means of the hydrogen–bubble method. It was then confirmed that the flow in the test-section was uniform in the same range of velocity except for the vicinity of the side-wall.

After the calibration, the water tunnel was slightly changed, that is, two nylon screens were changed to be removable, but it was experimentally confirmed that this change did not affect the flow quality in the test-section.

Fig. 5 shows the coordinate system of this experiment and Table 1 the experimental conditions of each visualization of the flow.
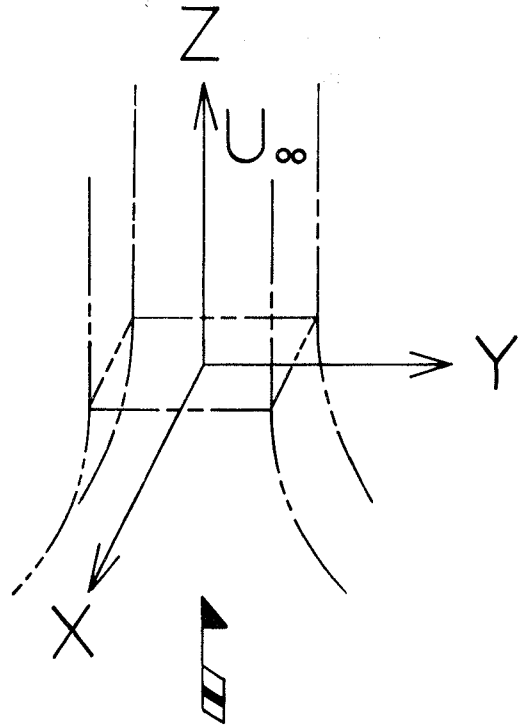


Fig. 5.  Coordinate system.

Table 1  Experimental conditions.

| Kind of visualization | Velocity of uniform flow (*mm/s*) | $X$ (*mm*) |
|---|---|---|
| Uniformity of the flow in the test–section | 10,    15,    50,    90 | 0, — 100 |
| The flow around a cylinder with injection | 20,    50 | 0 ∼ —100 |

In the experiment, $R_e$, $C_\mu$ and $\theta_J$ are independent variables and the observation was made at various combinations of them. The experiments were carried out in the symmetrical plane ($X = 0$ *mm*) and in the starboard sections of the cylinder ($X < 0$ *mm*).

## 5   Results and Discussion

5.1 Uniform flow in the test-section

The flow direction of the uniform flow in all plates is from the left to the right for convenience.
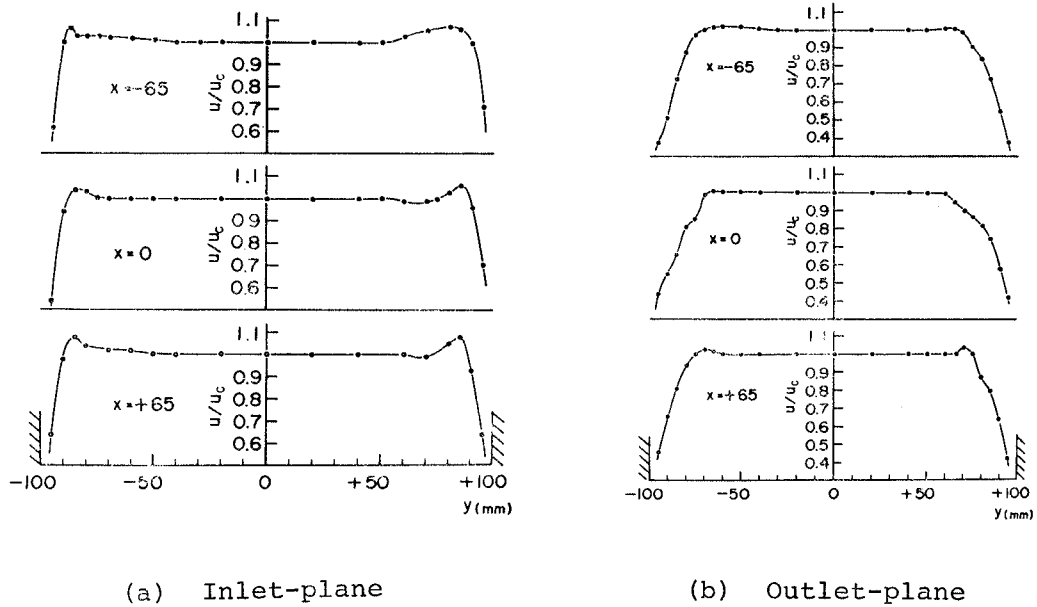


(a)   Inlet-plane                    (b)   Outlet-plane

Fig. 6.   Velocity distributions in the inlet- and outlet-planes of the test-section :
          $U_c = 11.1$ $mm/s$.

Figs. 6 (a) and (b) show the typical velocity distributions measured with the hydrogen-bubble method at the three spanwise positions in the inlet- and outlet-planes of the test-section, respectively, where $U_c$ indicates the velocity at the center of the test-section.   The increase of the velocity near the side-walls may have been caused by the curvature of the nozzle and the disks magnetically attached to the side-walls in order to tighten a platinum wire for the hydrogen-bubble method.
The boundary layer thicknesses of this case are about $15mm$ and about $40mm$ at the inlet- and the outlet-planes of the test-section, respectively.   It is found that the velocity distributions at $U_c = 90mm/s$ have the same tendency as at $U_c = 11.1mm/s$, but that at the higher velocity the boundary layer thickness at the outlet-plane is about $15mm$ and thinner, and that the uniformity of the flow is better.
  Figs. 7 (a), (b), (c) and (d) are the streamlines of the flow in the typical sections (at $X = 0$ $mm$ and $-100mm$) and at various $U_\infty$'s.   They show that the flow is laminar and almost perfectly parallel both at the center of the section and in the

(a)  $U_{\infty} = 15mm/s,\ X = 0\,mm$

(c)  $U_{\infty} = 10mm/s,\ X = -100mm$

(b)  $U_{\infty} = 90mm/s,\ X = 0\,mm$
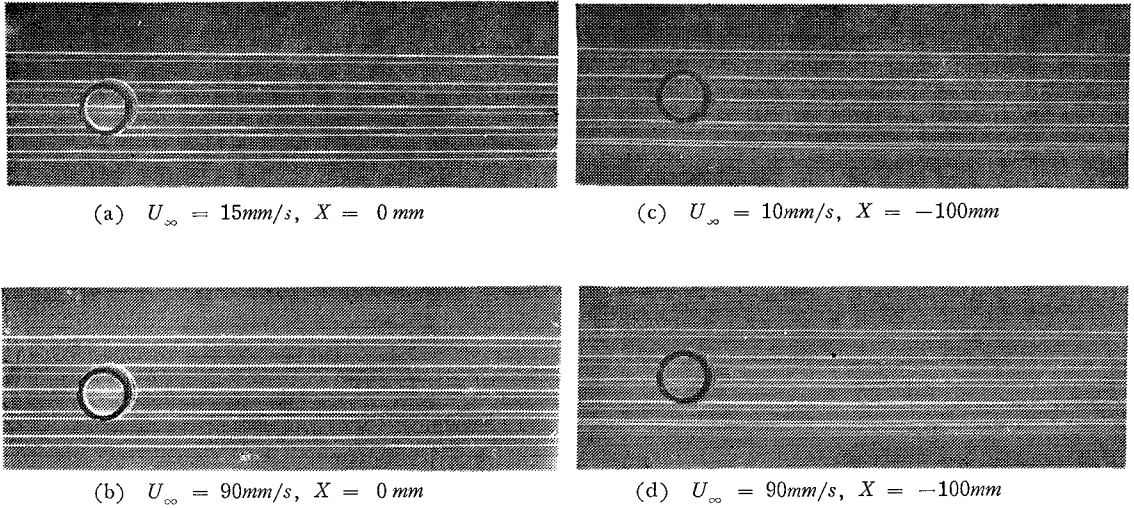
(d)  $U_{\infty} = 90mm/s,\ X = -100mm$

**Fig. 7.  Flows in the test-section.**

boundary layer. Thus, we conclude that this water tunnel is satisfactory to the flow visualization between the inlet- and the outlet-planes in the velocity range up to 90$mm/s$.

5.2 Flow around the cylinder in the symmetrical plane

Figs. 8 (a), (b), (c) and (d) show the flows around the cylinder in the symmetrical plane ($X = 0\ mm$) under the conditions that $R_{_e}$ and $\theta_{_J}$ are maintained constant



(a)  $C_{\mu} = 0$

(c)  $C_{\mu} = 2$
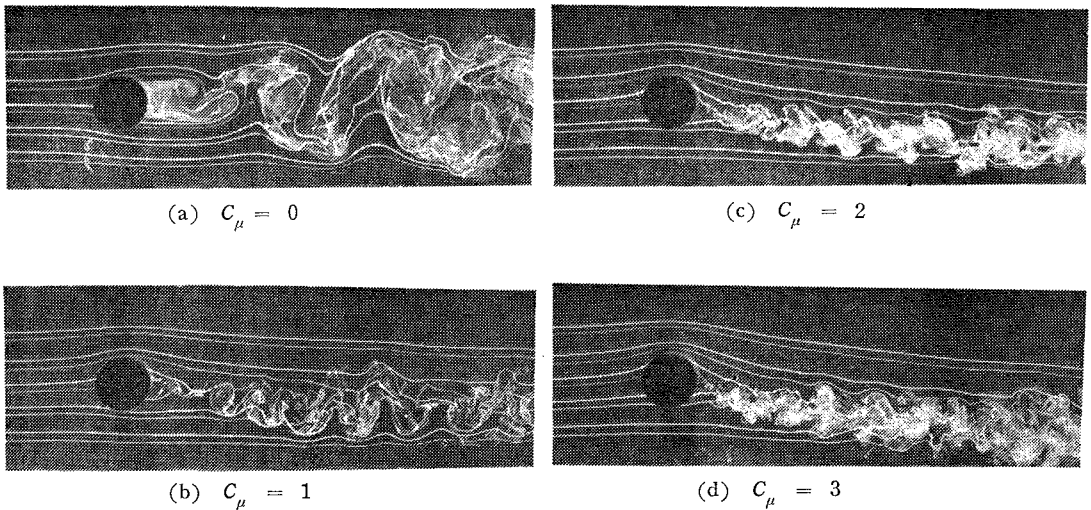
(b)  $C_{\mu} = 1$

(d)  $C_{\mu} = 3$

**Fig. 8.  Flows around the cylinder :** $R_{_e} = 926,\ \theta_{_J} = 0^{\circ}$.

to 926 and 0°, respectively,  and that $C_\mu$ is varied from 0 to 3.  It is seen from the
figures that,  as $C_\mu$ is increased, the upper and lower separation points, the stagnation
point and the streamlines around the cylinder  move  so as to increase the  circula-
tion around the cylinder. This was already described in detail in reference 2). Kár-
mán's vortex street is seen to be formed up in the  wake  though  it  is  incomplete,
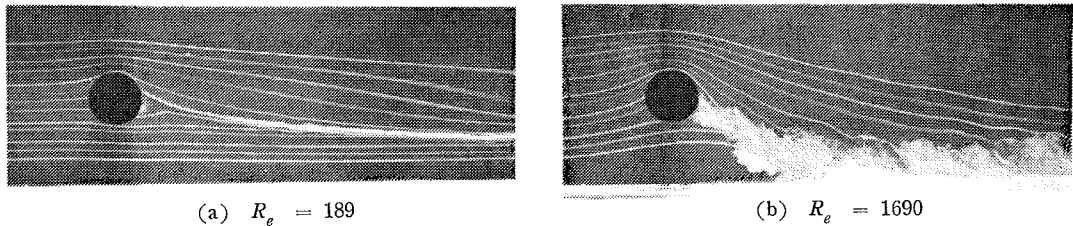and it is interesting that the street seems to be formed even  when  $C_\mu$  is 3.



(a)   $R_e$  = 189                                    (b)   $R_e$  = 1690

Fig. 9.   Flows around the cylinder : $C_\mu = 6$,  $\theta_J = 0°$.

The flows are shown in Figs. 9(a) and  (b) at two $R_e$'s ($R_e$  = 189 and  = 1690),
when $C_\mu$ and $\theta_J$ are maintained constant to 6 and 0°, respectively.  It  is  found  in
this case that the circulation around the cylinder is generated and is greater at the
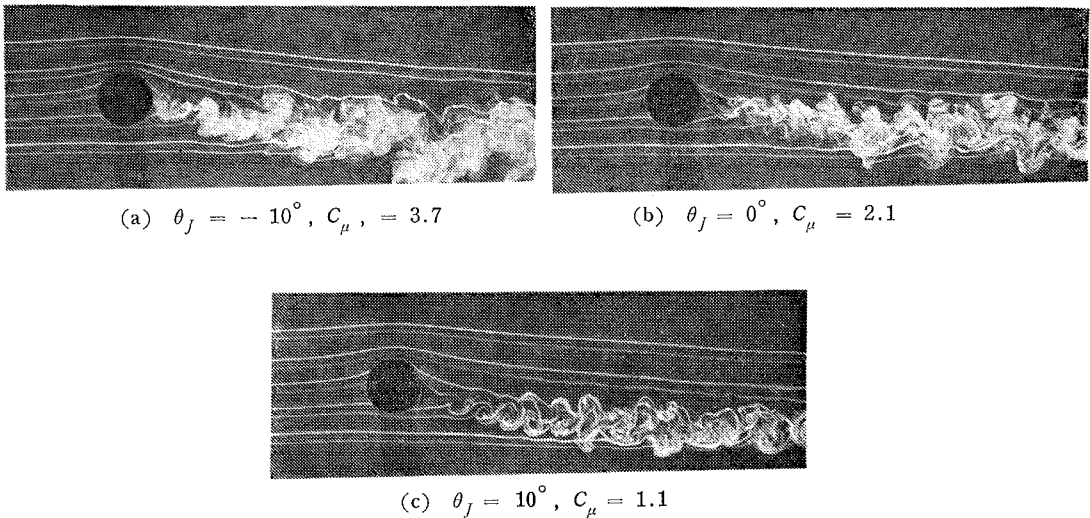larger $R_e$ , so that the lift acts on the cylinder.



(a)   $\theta_J = -10°$, $C_\mu$ , = 3.7                    (b)   $\theta_J = 0°$, $C_\mu$  = 2.1



(c)   $\theta_J = 10°$, $C_\mu = 1.1$

Fig. 10.   Flows around the cylinder having the same stagnation point : $R_e$ = 926.

Figs. 10 (a), (b) and (c) show the  flows  at $R_e$  = 926 in  which $C_\mu$ and $\theta_J$ are
adjusted so as to have the same stagnation  point.  The position  of  the  stagnation

point on the cylinder is determined by observation. The streamlines except the wake are almost alike although $\theta_J$ and $C_\mu$ are different. So, it is possible to obtain the flow which has nearly equal circulation.

### 5.3  Flow around the cylinder near the side-wall

We described hitherto the flow in the symmetrical plane only and the flow there was nearly two-dimensional. Next, we present the photographs of the flow at a few spanwise positions of the cylinder.
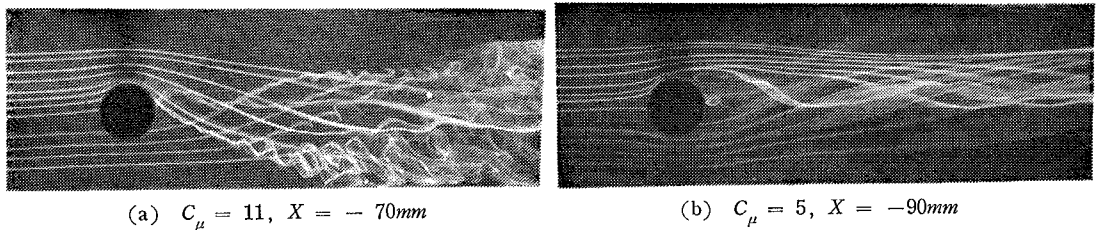


(a)  $C_\mu = 11, \ X = -70mm$          (b)  $C_\mu = 5, \ X = -90mm$

**Fig. 11.  Flows near the side-wall** : $R_e = 189, \ \theta_J = 0°$.

Figs. 11 (a) and (b) show the flows at $X = -70mm$ and $-90mm$, respectively. The streamlines of these figures are rolled up into the trailing vortex ; the streamlines of the lower side of the cylinder cross those of the upper side in such a way that this trailing vortex is rotating in the same sense as a right-handed screw advances downstream. Fig. 12 is a plate that the trailing vortex is shed downstream from the surface of the cylinder. Therefore, the downwash acts on the central part of the cylinder and the upwash on the cylinder in the region between the center of trailing vortex and the side-wall[1].

Fig. 13 is a photograph of a horseshoe vortex caused by the total pressure gradient in the spanwise direction near the stagnation point because of the boundary layer on the side-wall[3].



Fig. 12.  **Trailing vortex shed from the surface of the cylinder.**

The dyefilament is flowing away to both sides of the cylinder. Fig. 14 is the horseshoe vortex in the downstream. The vortex passing the upper side of the cylinder (the lift side) departs from the side-wall and is rolled up into the trailing vortex. The vortex to have passed the lower side creeps upward just on the side-wall and separates in two directions. One which flows downstream (rightward) continues
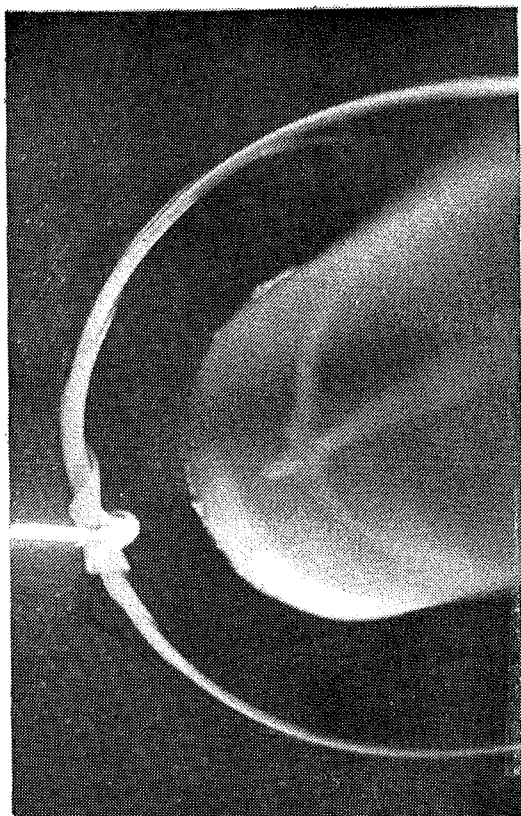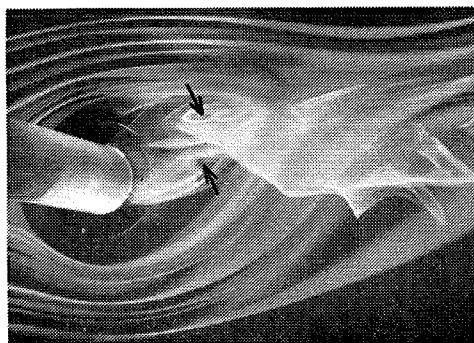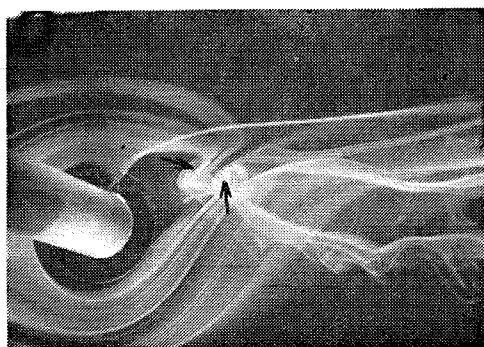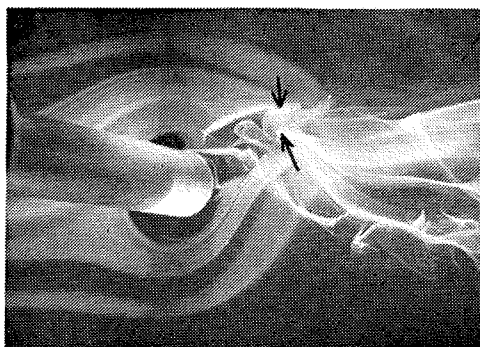
Fig. 13.   Horseshoe vortex.



Fig. 14.   Horseshoe vortex in the
           downstream.



(a)   $C_\mu = 3$



(b)   $C_\mu = 4.2$



(c)   $C_\mu = 5.4$

Fig. 15.   A pair of vortices on the side-wall : $R_e = 375$, $\theta_J = 0°$.

creeping and diverging on the surface. The other flows back upstream and is roll-
ed up into a pair of vortices described below.

Figs. 15 (a), (b) and (c) illustrate the two vortices formed on the side-wall just

behind the cylinder. The arrows in each plate indicate the cores of the vortices. Two vortices are formed as a pair, one in the upper and the other in the lower sides in the downstream of the cylinder, when $C_\mu = 0$ (not shown here).

The mechanism of the vortex formation may be thought qualitatively as follows (see Fig. 16) ; the vorticity vector of the side-wall boundary layer, $A$, is transported from far upstream and it is perpendicular to the main flow velocity vector. The flow, however, is accelerated near the upper- and lower-surfaces of the cylinder. Consequently, the vector $A$ is inclined against the main stream near the cylinder, that is, the vector $B$ has two components $B_1$ and $B_2$ . And, the streamwise vorticity component $B_2$ is stretched due to the acceleration and thus the vorticity is concentrated, so that a vortex is formed just behind the cylinder.
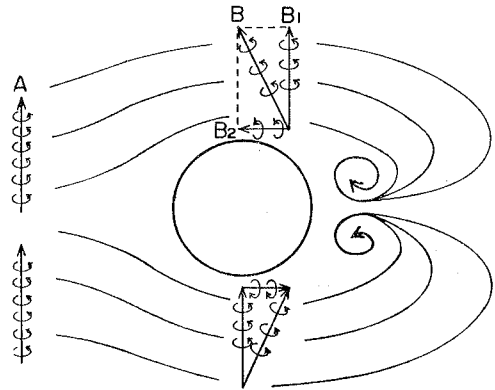


Fig. 16.   Mechanism of the formation of a pair of vortices on the side-wall.

As previously mentioned, the larger the $C_\mu$ is, the larger the upwash near the side-wall caused by trailing vortex is. Therefore, the two vortices on the side-wall move upward obliquely behind the cylinder (see Fig. 15).   These vortices have axes of the spanwise direction and depart from the side-wall. They are finally rolled up into the trailing vortex.

So far, we described three kinds of vortices, the first is a trailing vortex shed from the surface of the cylinder downstream, the second a horseshoe vortex and the third a pair of vortices on the side-wall. These vortices are all rolled up into one vortex, that is, a trailing vortex in the wake of the cylinder.

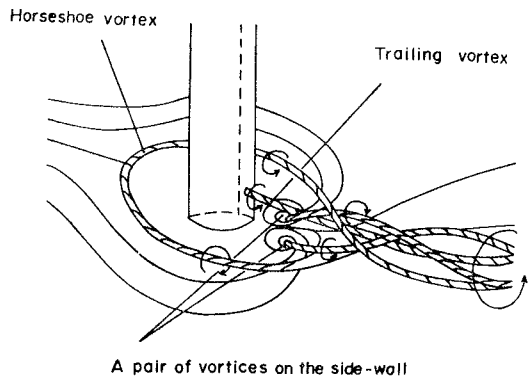The schematic view of the vortex system is illustrated in Fig. 17.



Fig. 17.   Structure of the vortex system.

## 6   Concluding remarks

We illustrated the flow pattern and the vortex system near the side-wall. The

three kinds of vortices roll up into one vortex, the so-called trailing vortex, and this flow pattern quite well explains the streamlines on the side-wall illustrated in Fig. 8 of the reference 1). Moreover, the result obtained in this flow visualization is consistent with the conclusions in reference 1).

### Reference

1) Yoshino and Waka, Reports of the Faculty of Engineering, Tottori University, **6-1** (1976-3), 1.

2) Yoshino and Waka, Reports of the Faculty of Engineering, Tottori University, **3-2** (1973-3), 25.

3) Thwaites, B., Incompressible Aerodynamics, (1960), 551, Oxford.